Journal of Biomechanics 49 (2016) 1794–1801

Contents lists available at ScienceDirect

Journal of Biomechanics

journal homepage: www.elsevier.com/locate/jbiomech
www.JBiomech.com

Cartilage loss patterns within femorotibial contact regions during deep knee bend ☆

J. Michael Johnson, Mohamed R. Mahfouz *

Department of Mechanical, Aerospace and Biomedical Engineering, University of Tennessee, Knoxville, TN 37996, USA

ARTICLE INFO

Article history:
Accepted 9 April 2016

Keywords:
Knee cartilage
Osteoarthritis
Kinematics
Statistical modeling
Cartilage degeneration

ABSTRACT

Osteoarthritis (OA) can alter knee kinematics and stresses. The relationship between cartilage loss in OA and kinematics is unclear, with existing work focusing on static wear and morphology. In this work, femorotibial cartilage maps were coupled with kinematics to investigate the relationship between kinematics and cartilage loss, allowing for more precise treatment and intervention. Cartilage thickness maps were created from healthy and OA subgroups (varus, valgus, and neutral) and mapped to a statistical bone atlas. Video fluoroscopy determined contact regions from 0° to 120° flexion. Varus and valgus subgroups displayed different wear patterns across the range of flexion, with varus knees showing more loss in early flexion and valgus in deeper flexion. For the femur, varus knees had more wear in the medial compartment than neutral or valgus and most wear at both 0° and 20° flexion. In the lateral femoral compartment, the valgus subgroup showed significantly more wear from 20° to 60° flexion as compared to other angles, though varus knees displayed highest magnitude of wear. For the tibia, most medial wear occurred at 0–40° flexion and most lateral occurred after 60° flexion. Knowing more about cartilage changes in OA knees provides insight as to expected wear or stresses on implanted components after arthroplasty. Combining cartilage loss patterns with kinematics allows for pre-surgical intervention and treatments tailored to the patient's alignment and kinematics. Reported wear patterns may also serve as a gauge for post-operative loading to be considered when placing implant components.

1. Introduction

Osteoarthritis (OA) of the knee brings about many changes in the affected joint, ranging from fluctuations in cartilage distribution, development of osteophytes, or subchondral edemas (Moskowitz et al., 2007). Ultimately, these changes are brought about by, and can lead to, abnormal kinematic motion. These kinematic changes alter the distribution of stresses on the articulating surface, often leading to suboptimal loading (Andriacchi et al., 2009). As the knee moves through the various degrees of flexion, the femorotibial contact regions progress from the central compartments of the femur surface to a posterior position (Komistek et al., 2003). It is likely that this contact pattern, and deviations from the described pattern, can give insight into degenerative changes in OA knees. Additionally, these contact regions, and cartilage loss within them, may give insight into expected implant wear patterns, specifically in TKA-utilizing procedures claiming restoration of natural kinematics.

In healthy subjects, the cartilage is thicker in regions that undergo the majority of stresses during normal gait (Koo et al., 2011). Furthermore, Li et al. (2005) showed that the cartilage-to-cartilage contact regions were associated with the thickest cartilage. Eckstein et al. (2008) and Wirth et al. (2009) further studied cartilage loss in the femorotibial joint in OA subjects by segmenting the cartilage plates and assigning regions for statistical analysis. The regions on the articulating surfaces, defined for the femur and the tibia, were located relative to manually selected landmarks as described in Eckstein et al. (2006a, 2006b). The findings by Wirth suggest that centrally located compartments of both joints undergo the majority of cartilage wear. While providing an excellent overview of cartilage loss, there are some shortcomings in the works of Wirth and Eckstein, such as poor resolution and reduced study reproducibility due to manually defined landmarks. One proposed method of high-resolution cartilage quantification across a population is through the use of statistical shape models (SSM), as first described by Cootes et al. (1995).

SSM for shape analysis is fairly common, as the 3D–3D landmark matching allows analogous morphological regions to be compared directly. Mahfouz (2012) have used high resolution SSM of the bony

☆All authors were fully involved in the study and preparation of the manuscript and that the material within has not been and will not be submitted for publication elsewhere.

* Correspondence to: Department of Mechanical, Aerospace and Biomedical Engineering, University of Tennessee, 307 Perkins Hall, 1506 Middle Drive, Knoxville, TN 37996, USA. Tel.: +1 865 974 7668.
E-mail address: mmahfouz@utk.edu (M.R. Mahfouz).

http://dx.doi.org/10.1016/j.jbiomech.2016.04.011

anatomy to perform morphological analyses across gender and ethnicities (Mahfouz et al., 2007). SSM of the bone can be used to drive the morphological cartilage analyses, not unlike Fripp et al. (2005), who used SSM for cartilage segmentation but not for degenerative morphology and Williams et al. (2010), who used a form of SSM for morphological analysis – but without a kinematic link. Kinematics were indirectly related to degenerative changes by Wirth et al. (2010) by spatially linking cartilage loss using angular femoral subregions.

In this work, a novel application of SSM is proposed for the purpose of cartilage thickness quantification of the femorotibial joint in healthy and pathological subjects from the Osteoarthritis Initiative, which is available for public access at http://www.oai.ucsf.edu/. The pathological dataset is combined with a kinematic contact analysis of healthy knees, using single plane X-ray video fluoroscopy (Komistek et al., 2003; Mahfouz et al., 2003, Leszko et al., 2011) with surface models having SSM point correspondence. While the motion data and cartilage data were derived from different subjects, the statistical atlas provides a framework for coupling the datasets. By integrating the cartilage model with kinematics *via* SSM correspondence, a link between cartilage wear and flexion angle can be established. This methodology can be applied to existing patient databases to provide high-resolution cartilage maps for degenerative subjects with point-to-point correspondence of cartilage loss for varying knee alignments. This framework for coupling *in vivo* cartilage loss with kinematic contact regions will allow for pre-surgical intervention and patient-specific treatment. It is expected that wear patterns will vary throughout the range of flexion and differ between joint space patterns.

2. Methods

2.1. Bone atlas

In order that we may model the cartilage layer across a population at sufficiently good spatial resolution, a statistical bone atlas is used to define point correspondence and anchor the cartilage layer to the bone. The atlas was created as outlined in previous works by Mahfouz et al. (2006). All data for the atlases were from healthy specimens segmented from CT with resolution of $0.625 \times 0.625 \times 0.625$ mm. For this work, separate atlases for the distal femoral component and proximal tibia component were used. The surface models for the femoral component contained $N=4120$ vertices and the tibia contained $N=4182$ vertices. The atlases were further split by gender, so that four atlases were used in total. The male femoral atlas was created from 199 healthy femurs, the female femoral atlas from 112 samples, the male tibia atlas from 89 samples, and female tibia atlas from 151 samples. Both male and female statistical atlases were created with identical point correspondence for each anatomy. Point correspondence, a non-trivial problem, was determined as outlined in Mahfouz et al. (2007) using a combination of registration and warping techniques. Given atlas correspondence, we seek to model cartilage relative to the bone surface as a list of bone vertices (the bone–cartilage interface [BCI]), mean cartilage thickness at each BCI vertex, and standard deviation of the thickness at each BCI vertex.

2.2. Cartilage dataset

Data for cartilage modeling was segmented from magnetic resonance imaging (MRI) datasets. All MRI data used in the preparation of this article were obtained from

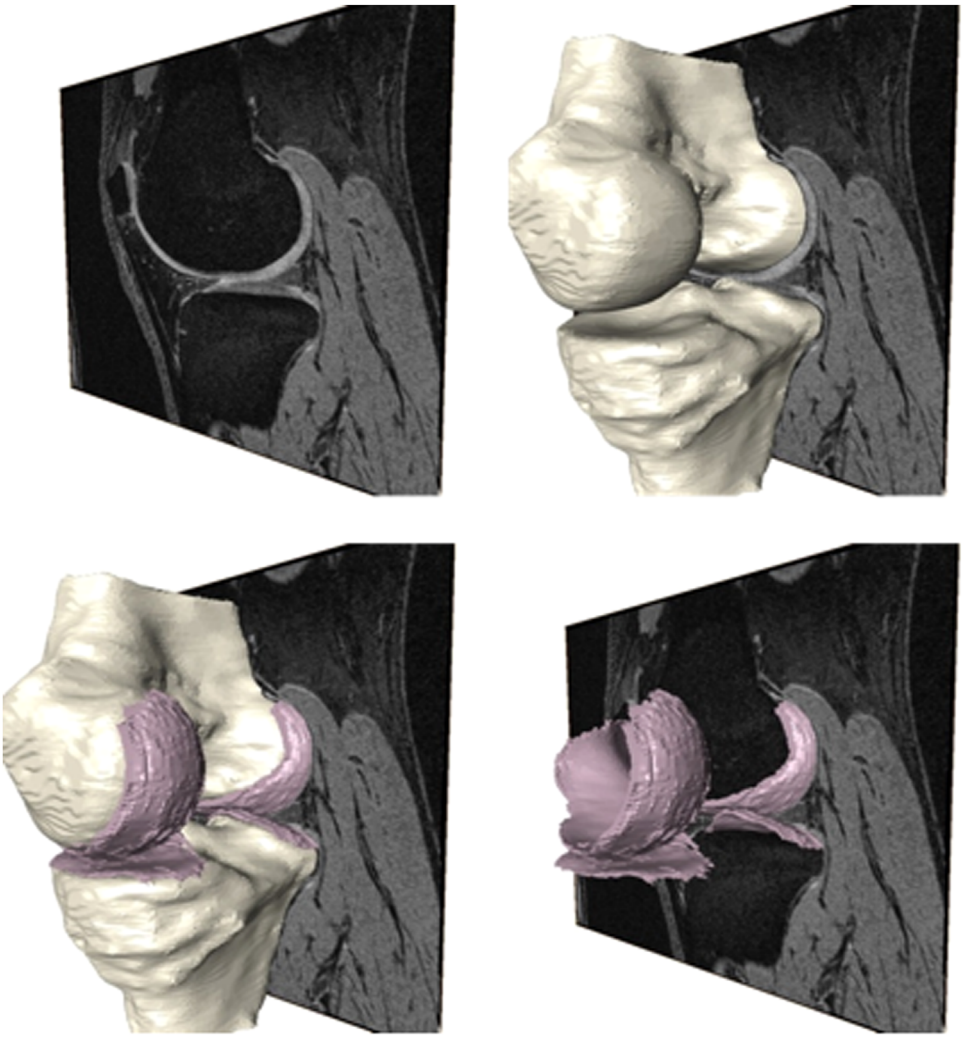

Fig. 1. Sample MRI image set (top left), bone segmentation (top right), cartilage segmentation (bottom right) and complete specimen (bottom left).

Table 1
Demographics for each cartilage grouping used in the study (A), including dataset sizes for male (B) and female (C) degenerative dataset by wear compartment and Kellgren-Lawrence (KL) score.

A. Healthy and degenerative male and female population demographics.

	Caucasian male (healthy)	Caucasian female (healthy)	Caucasian male (degenerative)	Caucasian female (degenerative)
Average age (years)	63	63	63	65
Age range (years)	47–76	45–77	48–78	46–78
Number right	26	30	19	19
Number left	14	10	3	7

B. Dataset sizes for male degenerative dataset by wear compartment & Kellgren–Lawrence score.

Male	**KL1**	**KL2**	**KL3**	**Total**
Varus	5	3	2	**10**
Valgus	2	1	5	**8**
Neutral	2	1	1	**4**
Total	**9**	**5**	**8**	**22**

C. Dataset sizes for the female degenerative dataset by wear compartment & KL score.

Male	**KL1**	**KL2**	**KL3**	**Total**
Varus	5	2	3	**10**
Valgus	2	4	4	**10**
Neutral	1	3	2	**6**
Total	**8**	**9**	**9**	**26**

the Osteoarthritis Initiative (OAI) database, which is available for public access at http://www.oai.ucsf.edu/. For all specimens included in this study, the sagittal double echo at steady state (DESS) images, having voxel size $0.365 \times 0.456 \times 0.7$ mm, were used for segmentation. For each knee image set, the femur, tibia, femoral cartilage and tibial cartilage were segmented using Avizo version 8.1.0 and verified by an expert having over 5 years of experience segmenting knee anatomies. Sample segmentation results can be seen in Fig. 1.

The dataset was divided into two main subgroups, healthy and pathological, by Kellgren–Lawrence (KL) grade. The pathological data (KL=1–3, as reported in OAI database) was further divided by compartment having the most joint space narrowing, namely medial, lateral or neutral joint space narrowing. A subset of the OAI healthy subgroup (KL=0) was used to establish baseline cartilage models. The healthy dataset contained 40 Caucasian males and 40 Caucasian females. Table 1 lists the demographics for each cartilage grouping used in the study (A), including dataset sizes for male (B) and female (C) degenerative dataset by wear compartment and Kellgren–Lawrence (KL) score.

2.3. Cartilage thickness model creation

The process of generating a cartilage model begins with segmented surface models of the bones and cartilage – a total of four surface models (femur bone, tibia bone, femur cartilage, and tibia cartilage). Segmentation of the OAI MRI scans results in a labeled volume, having 5 distinct intensities (0 for background, 1–4 for knee anatomy). From this labeled volume, the surface meshes are constructed from each non-background intensity value in Avizo version 8.1.0 using a marching cubes algorithm (Hege et al., 1997) and constrained smoothing extent of 5 to preserve surface normal directions. For the femur and tibia surfaces, the respective bone atlases are utilized to give the subject-specific meshes correspondence to the atlas as validated in Mahfouz et al. (2007).

In this work, cartilage is characterized by mean thickness and deviation at each vertex (location) on the osseous surface (BCI). Algorithm 1 (below) was used to extract femoral vertices and thicknesses belonging to the BCI for a single subject. The final BCI set was taken as the union of all subject-specific BCI sets. For the normal cohort, the union is intended to include all of the boundary cartilage points, which may vary slightly from subject-to-subject due to subject specific differences in bone geometry. In cases of total cartilage loss, some BCI points may be missing from those subjects.

The surface mesh is defined as a set of triangular faces. Each triangular face is comprised of three adjacent, connected vertices defining the face plane. The normal direction of each face is equivalent to the normal direction of the plane defined by the three vertices. The surface normal direction at each vertex, $\boldsymbol{n_i}$, is defined as the mean of the normal directions of each face containing the vertex. $I_c(s_i^d)$ denotes the intensity of the cartilage label volume (femoral cartilage for femur, tibial cartilage for tibia) at each sample location s_i^d (nearest voxel). Sampling was performed at 0.1 mm, which is sufficiently precise given the smallest voxel dimension of 0.365 mm.

Algorithm 1. BCI Set Creation.

```
1  i=0; BCI = {};
2  while (i < number of bone vertices)
3    for the bone vertex, v_i:
4      thickness(i)=0;
5      calculate surface normal direction at v_i, n_i;
6      distance d=0;
7      while (d <= 10 mm)
8        sample location s_i^d=v_i+n_i*d;
9        if (Cartilage label value I_c(s_i^d)!= 0)
10         if ( i ∉ BCI)
11         BCI = BCI ⋃ {i};
12         count(i)=count(i)+1;
13     end
14     thickness(i)=d;
15     end
16     d=d+0.1;
17     end
18     i++;
19end
```

Because all bone surface models have point correspondence with the respective bone atlas, the patient-specific results can be used in conjunction with the atlases to develop cartilage thickness statistics for a population. Thus, the thickness statistics for each cohort can be calculated at each vertex. For the healthy groups, the cartilage map is defined on the bone atlas as a list of vertices corresponding to the BCI and, at each vertex, the mean and standard deviation of the local cartilage thickness. The same was calculated for the degenerative datasets, though an additional statistic was generated: the mean degenerative thickness was normalized by the mean healthy thickness to provide an indication of average cartilage loss. The normalization of mean degenerated cartilage thickness is weighted at each vertex by the relative frequency of the vertex containing cartilage to avoid skewing the results to outlier values – primarily at the high curvature cartilage boundaries, where surface normal directions may be inconsistent.

2.4. Fluoroscopic dataset

In this work, kinematic data collected from normal subjects during deep knee bend was used to determine contact regions during the activity. For this study, five normal subjects performed deep knee bend under digital fluoroscopy. This data was previously analysed by Komistek et al. (2003). In that work, patient-specific bone models were segmented from computed tomography (CT) images and registered to frames in the digital fluoroscopy corresponding to flexion angles of 0°, 20°, 40°, 60°, 80°, 100° and 120°. All bones used in the fluoroscopic study were given atlas correspondence in order to couple the kinematic and cartilage data.

2.5. Contact model creation

From the fluoroscopic data, a contact model is sought. This contact model contains the atlas vertices that form the tibiofemoral contact region at each angle. The following method is used for extracting the contact vertices for a single subject from the fluoroscopic data. First, the femoral model is divided into medial and lateral vertices by a plane defined as passing through the mean point with normal direction calculated by the principal component of the bone model vertices closest to the medial–lateral direction. The divided set of vertices for a single subject can be seen in Fig. 2.

After division of the vertices, the atlas models are registered to each flexion angle using the transformations calculated from the 2D–3D fluoroscopic registration. For each flexion angle, the femoral contact vertices are calculated as the 5% of femoral vertices that have the smallest distance to the closest vertex of the tibia. This calculation is performed for both medial and lateral compartments. The contact vertices on the tibia are taken as the closest points on the tibia to each of the femoral contact vertices. After all subjects are analysed, the overall contact model is created at each flexion angle as the combination of all fluoroscopy subject contact

vertices. Fig. 3 shows the overall contact model at various flexion angles; the color scale reflects the probability that an atlas vertex will belong to the contact region. The probability that a vertex is a contact vertex was calculated as the number of times a vertex was included in the contact model divided by the total number of fluoroscopy subjects. Vertices with probability greater than 20% were used to analyze cartilage thickness within each region of contact.

2.6. Coupling cartilage and kinematics

The point correspondence of the atlas permits direct calculation of cartilage statistics in each contact region, allowing straightforward coupling of kinematic and cartilage data. As both cartilage and contact vertices are subsets of the list of bone vertices, the intersection of the cartilage model vertices and contact vertices at each angle were used to determine statistics for the cartilage thickness within each contact region. All statistics were weighted by contact probability. A flowchart of the process is shown in Fig. 4.

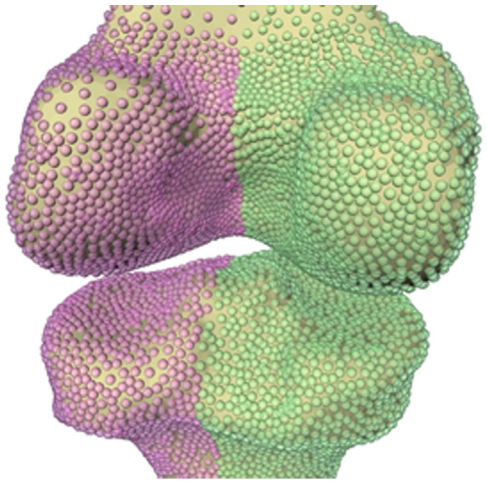

Fig. 2. Specimen with surface models divided into medial (green) and lateral (purple) vertices. (For interpretation of the references to color in this figure legend, the reader is referred to the web version of this article.)

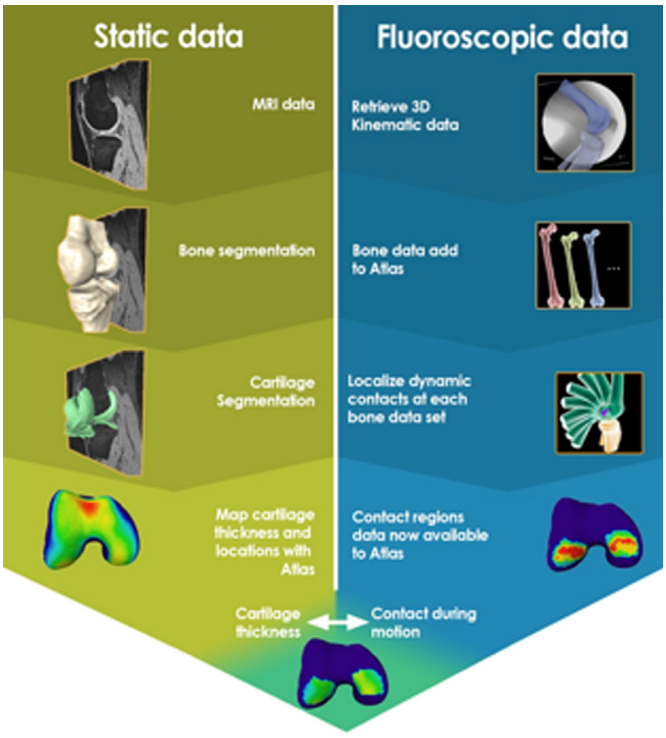

Fig. 4. Flowchart showing method of combining static and fluoroscopic data for analyzing cartilage loss within contact regions.

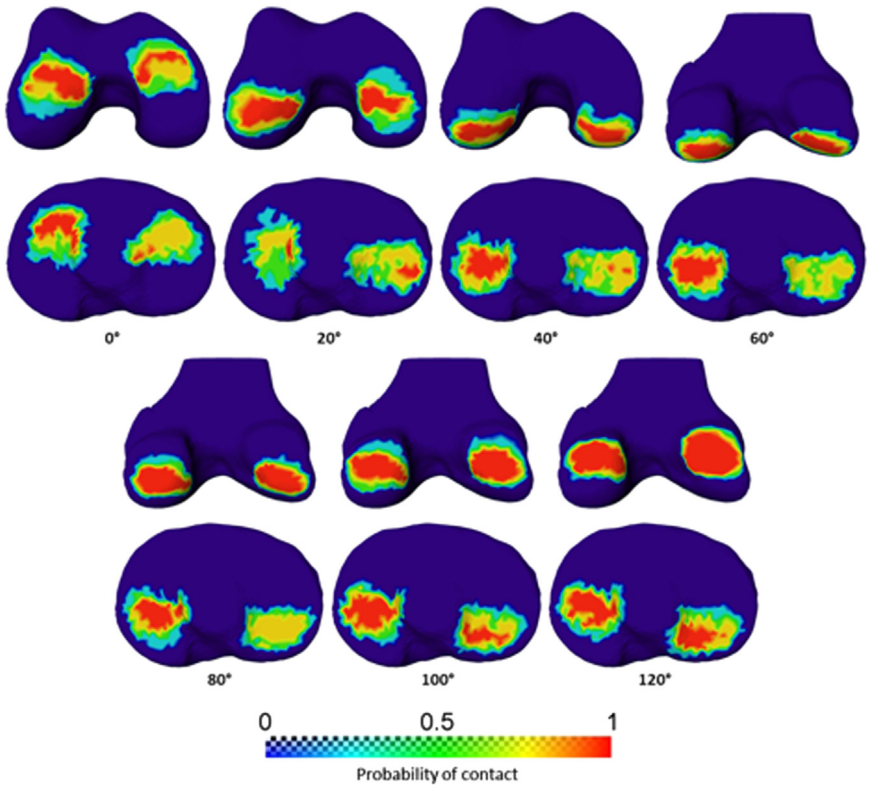

Fig. 3. Contact maps for various flexion angles during deep knee bend. Images show probability that an atlas vertex will belong to the contact region. (For interpretation of the references to color in this figure, the reader is referred to the web version of this article.)

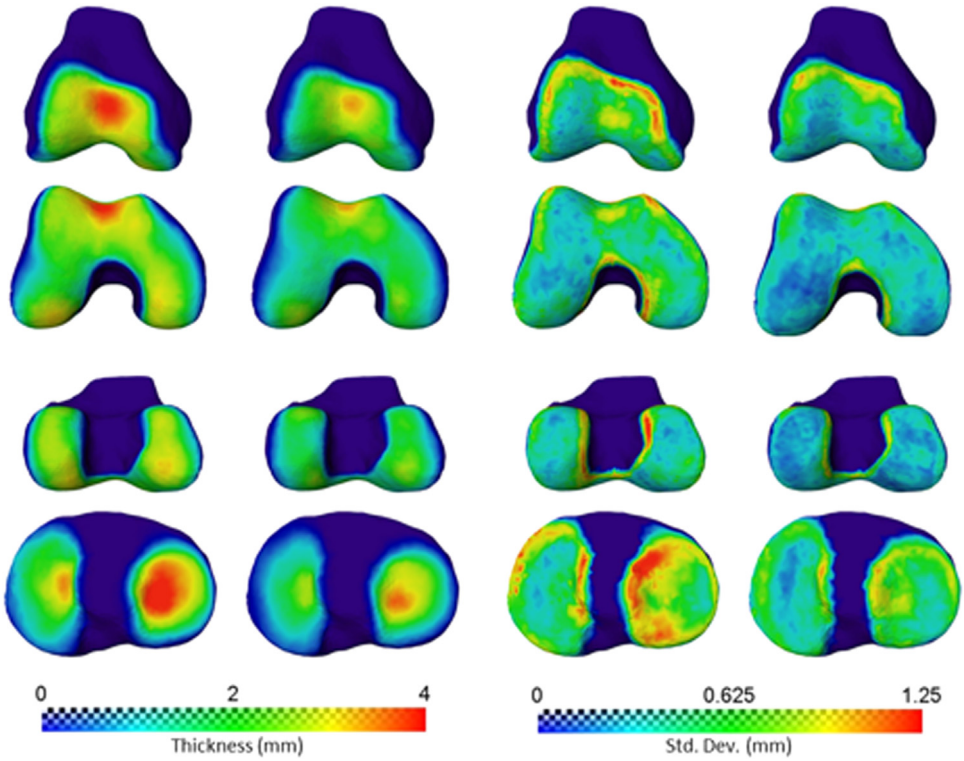

Fig. 5. Healthy cartilage thickness (left 2 columns) and standard deviation (right 2 columns) maps for male (left sub-columns) and females (right sub-columns) rendered on a template model from the statistical shape atlas.

2.7. Statistical methods

When multiple sets were compared, the Tukey–Kramer honest significant difference (HSD) was used due to the test's conservative properties when comparing unequal sample sizes, needed for comparing degenerative sets. The Wilcoxon rank-sum test was used to compare healthy groups – male *vs.* female and femur *vs.* tibia. The Wilcoxon test was chosen with the assumption that each comparison was between independent samples.

3. Results

3.1. Healthy cartilage models

Mean cartilage thickness for healthy male femur is 2.29 ± 0.68 mm and 2.04 ± 0.85 mm for the healthy male tibia. For the healthy female population, cartilage thickness is 1.91 ± 0.56 mm for the femur and 1.67 ± 0.70 mm for the tibia. Differences between femur and tibia were statistically significant for both males and females ($p < 0.001$). Male femoral and tibial cartilage was significantly thicker than female femoral and tibial cartilage respectively ($p < 0.001$). Fig. 5 shows surface renderings of the cartilage statistics.

3.2. Degenerative cartilage models

Mean cartilage thicknesses for degenerative femoral populations are 1.98 ± 0.59 mm, 1.88 ± 0.56 mm, 2.10 ± 0.59 mm for neutral, varus and valgus knees, respectively. This corresponds to normalized cartilage thicknesses of 0.97 ± 0.20, 0.91 ± 0.17, 0.96 ± 0.24. The varus cartilage layer is significantly thinner ($p < 0.001$) than both neutral and valgus, which have no significant differences between them as tested using Tukey–Kramer HSD.

For the tibia populations, mean cartilage thicknesses are 1.51 ± 0.63 mm, 1.54 ± 0.68 mm, 1.58 ± 0.57 mm for neutral, varus and valgus knees, respectively. Normalized thicknesses are 0.95 ± 0.33, 0.90 ± 0.23, and 0.84 ± 0.19. Comparison of means with Tukey–Kramer HSD shows significant differences between all groups ($p < 0.001$). High-resolution surface models showing cartilage thicknesses are shown in Fig. 6.

3.3. Cartilage in contact regions

For the femoral populations, the mean normalized thicknesses taken in all medial contact regions are 0.96 ± 0.36 for neutral, 0.84 ± 0.25 for varus, and 0.96 ± 0.30 for valgus. Varus was significantly thinner than the other two sets ($p < 0.001$), which have no significant difference between them. Within the lateral contact regions, the mean normalized thicknesses are 0.99 ± 0.39 for neutral, 0.89 ± 0.28 for varus and 0.97 ± 0.34 for valgus. For the lateral compartment, all differences are significant ($p < 0.001$).

In the medial tibia contact regions, mean normalized thicknesses are 0.83 ± 0.31 in neutral, 0.82 ± 0.21 in varus, and 0.96 ± 0.27 in valgus. Normalized thickness in the valgus knee is significantly greater than both neutral and varus ($p < 0.001$). Varus and neutral are not significantly different. In the lateral compartment, mean normalized thicknesses are 0.82 ± 0.25 in neutral, 0.85 ± 0.16 in varus and 0.73 ± 0.15 in valgus knees and all differences are significant ($p < 0.001$).

Among all groups, the contact region at 0° has significantly higher normalized cartilage thickness, 0.92 ± 0.33 compared to 0.81 ± 0.16 at the next thickest region (20°, $p < 0.001$). This is the only contact region on femur or tibia which is significantly different amongst all groups.

For neutral knees, the greatest femoral loss occurs at 40° flexion in the medial femur. The difference in this thickness and all other femoral thicknesses in the neutral knee is significantly different. Normalized tibia wear occurs most in the medial compartment at 20° flexion, though this is not significantly different ($p > 0.05$) from fractional thickness at 100° or 120° in the lateral

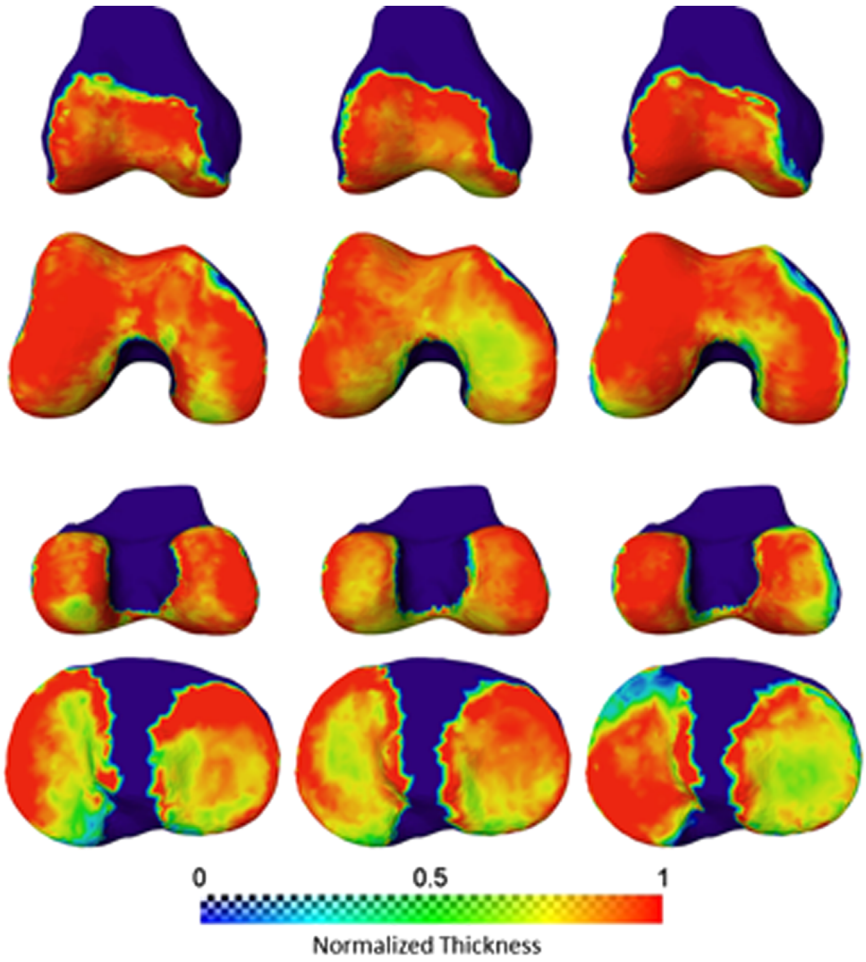

Fig. 6. Normalized thickness (by healthy means) maps for degenerative cartilage in neutral (left column), varus (center column) and valgus (right column) knees.

compartment. Table 2 shows normalized cartilage thickness in each contact region for neutral, varus and valgus alignments, respectively.

In varus knees, normalized femoral cartilage thickness has a minimum of 0.77 in the medial compartment at both 0° ($\pm$0.17) and 20° ($\pm$0.18) flexion. These two regions are not significantly different from one another, but both are significantly different from all other contact regions. In the tibia, thinnest normalized cartilage thickness is seen in the lateral compartment at 100° flexion, though this is not significantly different from values in several other contact regions (lateral 80°, lateral 120°, medial 20–120°).

In valgus knees, the femoral cartilage has minimum normalized thickness of 0.89 ± 0.22 at 40° flexion, though this is not significantly different than values at 20° and 60°. The tibia exhibits more relative wear, with minimum normalized thickness of 0.71 at 60–100° flexion.

4. Discussion

In this work, cartilage wear patterns were coupled with kinematics using statistical atlases for novel understanding of the relationship between cartilage loss and femorotibial contact. Point correspondence properties of the atlases were utilized to map contact regions during deep knee bend as well as cartilage thickness statistics for representative bone anatomies. The process presented in this work achieves multiple end objectives: outlining a reproducible, high-resolution method for mapping cartilage and cartilage loss, using atlases to perform cartilage statistical analyses, and coupling atlases and kinematics in a way that provides new insight into cartilage loss as it relates to kinematics.

The primary objective of this work is to introduce a method for creating high-resolution cartilage maps for degenerative subjects. Previous methods investigating degenerative cartilage changes in subregions of the cartilage plates use anatomically defined landmarks as reference (Eckstein et al., 2006a, 2006b; Wirth et al., 2009, 2011), whereas this work proposes a methodology for high-resolution sampling and analysis of femorotibial cartilage thickness. The work by Williams et al. (2010) is especially comparable, though the maximum cartilage thickness reported in their work was quite high, nearly 2.5 cm. The overall cartilage distributions for asymptomatic populations achieved through this study generally agree with work by Williams et al. (2010) and with other existing literature (Fripp et al., 2010). This is the first known work to provide point-to-point correspondence of cartilage loss for neutral, varus and valgus knee alignments.

A secondary objective of this work is to introduce a framework for coupling *in vivo* cartilage loss with kinematic contact regions. This unique utilization of the point-correspondence properties of the statistical bone atlas may allow further refinement of the angular compartments presented by Wirth et al. (2010), in that contact regions may be more clinically relevant. Despite only including deep knee bend in this analysis, it is likely that early flexion angles presented here are relevant to regions indicative of gait (the predominant activity for most subjects). These early flexion (20–40°) and extension (0°) regions correspond to areas of high cartilage wear in varus knees, although we see deep flexion angles ($>40°$) corresponding to higher loss in the tibia, especially

Table 2
Normalized cartilage thickness for neutral (A), varus (B), and valgus (C) alignments.

Flexion angle (deg)	Medial femur	Lateral femur	Medial tibia	Lateral tibia
A. Neutral OA compartments				
0	0.97 ± 0.26	1.04 ± 0.33	0.82 ± 0.40	0.98 ± 0.48
20	0.95 ± 0.44	0.94 ± 0.17	0.77 ± 0.19	0.82 ± 0.15
40	0.90 ± 0.43	0.95 ± 0.21	0.82 ± 0.27	0.81 ± 0.12
60	0.98 ± 0.36	0.99 ± 0.31	0.83 ± 0.29	0.80 ± 0.12
80	1.01 ± 0.31	1.00 ± 0.23	0.83 ± 0.31	0.80 ± 0.13
100	0.97 ± 0.30	1.01 ± 0.29	0.86 ± 0.34	0.78 ± 0.13
120	0.92 ± 0.34	1.02 ± 0.43	0.84 ± 0.31	0.79 ± 0.17
B. Varus OA compartments				
0	0.77 ± 0.17	0.90 ± 0.17	0.84 ± 0.32	0.94 ± 0.16
20	0.77 ± 0.18	0.89 ± 0.21	0.82 ± 0.20	0.87 ± 0.11
40	0.84 ± 0.16	0.89 ± 0.15	0.81 ± 0.17	0.85 ± 0.12
60	0.85 ± 0.20	0.92 ± 0.17	0.81 ± 0.16	0.84 ± 0.11
80	0.86 ± 0.27	0.90 ± 0.22	0.82 ± 0.17	0.82 ± 0.12
100	0.88 ± 0.28	0.87 ± 0.36	0.82 ± 0.19	0.80 ± 0.13
120	0.87 ± 0.36	0.89 ± 0.51	0.81 ± 0.18	0.81 ± 0.20
C. Valgus OA compartments				
0	0.90 ± 0.29	1.06 ± 0.20	0.88 ± 0.38	0.82 ± 0.19
20	0.94 ± 0.23	0.94 ± 0.24	0.92 ± 0.28	0.73 ± 0.10
40	0.97 ± 0.22	0.89 ± 0.22	0.97 ± 0.23	0.72 ± 0.10
60	0.98 ± 0.23	0.91 ± 0.29	0.99 ± 0.21	0.71 ± 0.09
80	0.96 ± 0.33	0.98 ± 0.33	0.98 ± 0.23	0.71 ± 0.09
100	0.99 ± 0.31	1.02 ± 0.41	0.99 ± 0.23	0.71 ± 0.11
120	0.94 ± 0.44	0.98 ± 0.49	0.97 ± 0.23	0.73 ± 0.21

in the lateral compartment. One clue to higher magnitude wear on the posterior-lateral aspect of the tibia could be that during deep flexion angles, loading on the tibia is at a maximum (Kutzner et al., 2010), even if this flexion angle is not experienced as often during regular daily activity. OA changes may further increase susceptibility for cartilage wear in this high-load region of flexion.

Limitations of this work include a relatively small sample size for each degenerative patient group. This was due mainly to the relatively lengthy segmentation process. The sample size of 128 analysed subjects leads to statistically significant results and thus represents a sufficient patient population for evaluating the process. A second, less critical weakness lies in the inherent sampling of the bone surfaces. For the triangulated surface meshes, the cartilage boundaries often lay in regions of high curvature. The surface sampling may not be adequate in these regions, leading to artificially high variation in measured cartilage thicknesses. As the main concern of this work is cartilage thickness within contact regions, errors within these high curvature regions have little effect on reported results. Another limitation is the discrepancy between contact on healthy subjects and cartilage on degenerative subjects. The fluoroscopic data did not include cartilage, the inclusion of which may alter detected contact areas though the effect is likely minimal given the conformal nature of the cartilage pads. It is also unclear how Osteoarthritis and knee malalignment will affect the contact paths and regions, but conducting MRI and kinematic analysis for a sufficient osteoarthritic population would be a significant research study, possibly unrealistic given expected pain tolerances and reduced ROM of subjects with higher KL grades.

Ideally, individualized reported wear patterns can help guide patient treatment options in a way that prevents loading on regions susceptible to wear. The loss pattern suggests a strategy of reducing load in the medial compartment during early flexion and in the lateral compartment during deeper flexion. The flexion regions of maximal wear differ depending on knee alignment, suggesting alignment may indicate different load-reducing treatment pathways. Characterization of cartilage loss patterns and methods of coupling loss with biomechanics has important implications in multiple areas: implant design, treatment pathways, preventative measures, and novel treatment devices. Implications for implant components may depend on reported wear patterns and consideration of post-operative loading. This work provides both a method for creating high-resolution cartilage maps for degenerative subjects with point-to-point correspondence of cartilage loss for varying knee alignments and a framework for coupling *in vivo* cartilage loss with kinematic contact regions, allowing for pre-surgical intervention and patient-specific treatment.

Conflict of interest statement

I, Mohamed R. Mahfouz, corresponding author, have nothing to disclose regarding a conflict of interest for this original article submission under consideration for publication. There are no relevant conflicts of interest for financial activities, personal relationship, or intellectual property claims. Likewise, author J. Michael Johnson has nothing to disclose regarding a conflict of interest. There are no relevant conflicts of interest for financial activities, personal relationship, or intellectual property claims.

Acknowledgments

The authors would like to thank Dr. Gary To for graphic assistance, Wesley Underwood for data organization, Dr. Emam Elhak Abdel Fatah for kinematic support, Jayne Dadmun for technical writing and Lyndsay Bowers for administrative support. The OAI is a public–private partnership comprised of five contracts (N01-AR-2-2258; N01-AR-2-2259; N01-AR-2-2260; N01-AR-2-2261; N01-AR-2-2262) funded by the National Institutes of Health, a branch of the Department of Health and Human Services, and conducted by the OAI Study Investigators. Private funding partners include Merck Research Laboratories; Novartis Pharmaceuticals Corporation, GlaxoSmithKline; and Pfizer, Inc. Private sector funding for the OAI is managed by the Foundation for the National Institutes of Health. This manuscript was prepared using an OAI public-use data set and does not necessarily reflect the opinions or views of the OAI investigators, the NIH, or the private funding partners.

References

Andriacchi, T.P., Koo, S., Scanlan, S.F., 2009. Gait mechanics influence healthy cartilage morphology and osteoarthritis of the knee. J. Bone Jt. Surg. – Am. 91 (Suppl. 1), 95–101. http://dx.doi.org/10.2106/JBJS.H.01408.

Cootes, T.F., Taylor, C.J., Cooper, D.H., Graham, J., 1995. Active shape models – their training and application. Comput. Vis. Image Underst. 61 (1), 38–59.

Eckstein, F., Burstein, D., Link, T.M., 2006a. Quantitative MRI of cartilage and bone: degenerative changes in osteoarthritis. NMR Biomed. 19 (7), 822–854.

Eckstein, F., Wirth, W., Hudelmaier, M., Stein, V., Lengfelder, V., Cahue, S., Marshall, M., Prasad, P., Sharma, L., 2008. Patterns of femorotibial cartilage loss in knees with neutral, varus, and valgus alignment. Arthritis Care Res. 59 (11), 1563–1570.

Eckstein, F., Ateshian, G., Burgkart, R., Burstein, D., Cicuttini, F., Dardzinski, B., Gray, M., Link, T.M., Majumdar, S., Mosher, T., Peterfy, C., Totterman, S., Waterton, J., Winalski, C.S., Felson, D., 2006b. Proposal for a nomenclature for magnetic resonance imaging based measures of articular cartilage in osteoarthritis. Osteoarthr. Cartil. 14 (10), 974–983.

Fripp, J., Crozier, S., Warfield, S.K., Ourselin, S., 2010. Automatic segmentation and quantitative analysis of the articular cartilages from magnetic resonance images of the knee. IEEE Trans. Med. Imaging 29 (1), 55–64. http://dx.doi.org/10.1109/TMI.2009.2024743.

Fripp, J., Bourgeat, P., Mewes, A.J., Warfield, S.K., Crozier, S., Ourselin, S., 2005. 3D statistical shape models to embed spatial relationship information. In: Proceedings of the 1st International Workshop on Computer Vision for Biomedical Image Applications. Beijing, China, 1, pp. 51–60.

Hege, H.-C., Seebass, M., Stalling, D., Zockler, M., 1997. A generalized marching cubes algorithm based on non-binary classifications. Preprint SC 97-05, Konrad-Zuse-Zentrum für Informationstechnik, Berlin, Germany.

Komistek, R.D., Dennis, D.A., Mahfouz, M., 2003. In vivo fluoroscopic analysis of the normal human knee. Clin. Orthop. Relat. Res. 410, 69–81.

Koo, S., Rylander, J.H., Andriacchi, T.P., 2011. Knee joint kinematics during walking influences the spatial cartilage thickness distribution in the knee. J. Biomech. 44 (7), 1405–1409.

Kutzner, I., Heinlein, B., Graichen, F., Bender, A., Rohlmann, A., Halder, A., Beier, A., Bergmann, G., 2010. Loading of the knee joint during activities of daily living measured in vivo in five subjects. J. Biomech. 43 (11), 2164–2173.

Leszko, F., Hovinga, K.R., Lerner, A.L., Komistek, R.D., Mahfouz, M.R., 2011. In vivo normal knee kinematics: is ethnicity or gender an influencing factor? Clin. Orthop. Relat. Res. 469 (1), 95–106.

Li, G., Park, S.E., DeFrate, L.E., Schutzer, M.E., Ji, L., Gill, T.J., Rubash, H.E., 2005. The cartilage thickness distribution in the tibiofemoral joint and its correlation with cartilage-to-cartilage contact. Clin. Biomech. 20 (7), 736–744.

Mahfouz, M., Merkl, B., Abdel Fatah, E., Booth Jr., R., Argenson, J., 2007. Automatic methods for characterization of sexual dimorphism of adult femora: distal femur. Comput. Methods Biomech. Biomed. Eng. 10 (6), 447–456.

Mahfouz, M.R., 2012. Three-dimensional morphology of the knee. In: Scott, W.N. (Ed.), Insall & Scott Surgery of the Knee. Churchill Livingstone (Elsevier), Philadelphia, p. 142.

Mahfouz, M.R., Hoff, W.A., Komistek, R.D., Dennis, D.A., 2003. A robust method for registration of three-dimensional knee implant models to two-dimensional fluoroscopy images. IEEE Trans. Med. Imaging 22 (12), 1561–1574. http://dx.doi.org/10.1109/TMI.2003.820027.

Mahfouz, M., Badawi, A., Merkl, B., Fatah, E.E.A., Pritchard, E., Kesler, K., Moore, M., Jantz, R., 2006. 3D statistical shape models of patella for sex classification. In: Proceedings of the 28th Annual International Conference of the IEEE Engineering in Medicine and Biology Society, EMBS'06. New York, NY, USA, pp. 3439–3445. ⟨http://dx.doi.org/10.1109/IEMBS.2006.259373⟩.

Moskowitz, R.W., Altman, R.D., Hochberg, M.C., Buckwalter, J.A., Goldberg, V.M., 2007. Osteoarthritis: Diagnosis and Medical/Surgical Management. Lippincott Williams & Wilkins, Philadelphia.

Williams, T.G., Holmes, A.P., Waterton, J.C., Maciewicz, R.A., Hutchinson, C.E., Moots, R.J., Nash, A.F.P., Taylor, C.J., 2010. Anatomically corresponded regional analysis of cartilage in asymptomatic and osteoarthritic knees by statistical shape modelling of the bone. IEEE Trans. Med. Imaging 29 (8), 1541–1559.

Wirth, W., Benichou, O., Kwoh, C.K., Guermazi, A., Hunter, D., Putz, R., Eckstein, F., 2010. Spatial patterns of cartilage loss in the medial femoral condyle in osteoarthritic knees: data from the osteoarthritis initiative. Magn. Reson. Med. 63 (3), 574–581.

Wirth, W., Hellio Le Graverand, M.-P., Wyman, B.T., Maschek, S., Hudelmaier, M., Hitzl, W., Nevitt, M., Eckstein, F., 2009. Regional analysis of femorotibial cartilage loss in a subsample from the osteoarthritis Initiative progression subcohort. Osteoarthr. Cartil. 17 (3), 291–297.

Wirth, W., Buck, R., Nevitt, M., Le Graverand, M.P., Benichou, O., Dreher, D., Davies, R.Y., Lee, J.H., Picha, K., Gimona, A., Maschek, S., Hudelmaier, M., Eckstein, F., 2011. MRI-based extended ordered values more efficiently differentiate cartilage loss in knees with and without joint space narrowing than region-specific approaches using MRI or radiography – data from the OA initiative. Osteoarthr. Cartil. 19 (6), 689–699.